Thoracic Cancer

WILEY

ORIGINAL ARTICLE OPEN ACCESS

ATF3 Within the Interferon Signaling Pathway: A Potential Biomarker for Predicting Pathological Response to Neoadjuvant Chemoimmunotherapy

Chao He[1] | Rui Han[1,2] | Taiming Zhang[1,3] | Peng Zhong[1,4] | Daijuan Huang[1] | Conghua Lu[1] | Yimin Zhang[1] | Jianghua Li[1,2] | Yuwen Deng[1,4] | Yong He[1]

[1]Department of Respiratory Disease, Daping Hospital, Army Medical University, Chongqing, China | [2]Department of Respiratory Disease, Bishan Hospital of Chongqing Medical University, Bishan Hospital of Chongqing, Chongqing, China | [3]Department of Thoracic Surgery, Daping Hospital, Army Medical University, Chongqing, China | [4]Department of Pathology, Daping Hospital, Army Medical University, Chongqing, China

Correspondence: Yong He (heyong@tmmu.edu.cn)

Received: 10 February 2025 | **Revised:** 12 March 2025 | **Accepted:** 19 March 2025

Funding: This work was supported by Chongqing Municipal Bureau of Science and Technology, cstc2021jscx-xczxX0015; National Natural Science Foundation of China, Grant Nos.82473226; Chongqing Technology Innovation and Application Development Special Key Project, CSTB2023TIAD-STX0003.

Keywords: ATF3 | biomarkers | chemoimmunotherapy | IFN signaling pathway | NSCLC | pathological response

ABSTRACT

Background: Neoadjuvant chemoimmunotherapy has achieved high downstaging and pathologic response rates in nonsmall-cell lung cancer (NSCLC), but outcomes vary significantly. Early identification of beneficiaries remains a challenge.

Methods: This study analyzed baseline transcriptomic data from 24 NSCLC patients (9 major pathological response [MPR], 15 nonmajor pathological response [NMPR]) treated with neoadjuvant chemoimmunotherapy, sourced from the GEO database. Molecular analyses and immune infiltration analyses were performed using pathologic response as an endpoint. After identifying the interferon signaling subset NeoIGS, we analyzed the relationship between NeoIGS and immune scores, immune cell infiltration, and immunotherapy efficacy. A key gene in NeoIGS was screened by reveiver operating characteristic curve (ROC) analysis. Subsequently, the expression of the key gene was assessed by immunohistochemistry in 53 NSCLC patients receiving neoadjuvant chemoimmunotherapy.

Results: Interferon signaling pathway expression and CD8+ T-cell infiltration were higher in the MPR group. NeoIGS predicted pathological response to neoadjuvant chemoimmunotherapy (AUC = 0.926) and also demonstrated predictive value in the ICIs monotherapy cohort. IPS and TIDE scores also confirmed NeoIGS's association with immunotherapy in the TCGA NSCLC dataset. Furthermore, patients with higher NeoIGS scores had more immune cell infiltration and increased expression of ICI targets. ROC analysis identified ATF3 as NeoIGS's key gene. In the clinical cohort, ATF3 outperformed PD-L1 in predicting pathologic response, with a 90.0% MPR rate in the high-expression group.

Conclusion: We established that a subset of interferon signaling pathways, NeoIGS, is closely associated with immunotherapy. Among them, ATF3 is the most critical gene that accurately predicts pathological remission in neoadjuvant chemoimmunotherapy.

Chao He and Rui Han contributed equally to this work.

1 | Introduction

Lung cancer is the leading cause of cancer morbidity and mortality, resulting in a heavy social burden and significant economic losses [1]. Nonsmall-cell lung cancer (NSCLC) is the most common type of lung cancer, accounting for 85% of all cases [2]. Despite significant advances in cancer treatment, the clinical outcome of NSCLC remains far from satisfactory [2, 3]. Recently, immune checkpoint inhibitors (ICIs) have shown promising efficacy in patients with NSCLC, improving clinical prognosis and inducing durable remissions, especially in patients with good response [4–6]. Studies have shown that ICIs can be safely and effectively used in combination with cytotoxic chemotherapy, making combination therapy the standard of therapy for most NSCLC patients [7]. However, it is undeniable that even with the use of chemotherapy combined with immunotherapy, a large proportion of patients still do not achieve good clinical outcomes, especially in neoadjuvant therapy [8, 9].

Biomarkers such as PD-L1 expression and tumor mutational load (TMB) have been widely used to predict the effectiveness of anti-PD-1/PD-L1 therapy. High PD-L1 expression is generally associated with better outcomes in patients receiving anti-PD-1 monotherapy [10, 11]. In addition, numerous clinical trials have shown that patients exhibiting high TMB derive greater therapeutic benefit from anti-PD-1/PD-L1 immunotherapy compared to conventional chemotherapy [12–14]. However, a growing number of clinical trials have shown that neither PD-L1 expression nor TMB levels are effective predictors of the efficacy of chemotherapy in combination with ICIs [15–18]. Therefore, it is imperative to identify biomarkers that can predict the efficacy of chemoimmunotherapy.

Currently, a substantial body of research exploring predictive biomarkers for immunotherapy efficacy primarily employs assessments based on CT imaging as indicators of short-term treatment outcomes. Nevertheless, this methodology may be considered unreliable owing to the potential incidence of pseudoprogression as a result of immunotherapy [19]. In contrast, the assessment of pathological responses in resected specimens offers a more objective metric for determining therapeutic efficacy. Moreover, studies have shown a significant correlation between increased pathological response and improved survival outcomes in patients with resectable NSCLC following neoadjuvant chemoimmunotherapy [20, 21]. Therefore, this study selects pathological response as a treatment outcome to more accurately explore predictive biomarkers for the efficacy of chemoimmunotherapy.

In this study, we retrospectively analyzed pretreatment transcriptomic profiles of patients receiving neoadjuvant chemoimmunotherapy to identify expression signatures associated with pathologic response. We developed interferon signaling-related features, termed NeoIGS, to predict treatment efficacy in NSCLC patients. Comprehensive evaluations were performed to explore interrelationships among immune scores, immune cell infiltration, and NeoIGS. In addition, we identified the most predictive genes using subject receiver operating characteristic (ROC) curve analysis. To corroborate these findings, pretreatment biopsy samples from 53 patients undergoing neoadjuvant chemoimmunotherapy were analyzed. Protein expression, pathologic response, and prognosis were further assessed using immunohistochemical staining.

2 | Materials and Methods

2.1 | Data Collection

To investigate tumor characteristics related to the pathological response to chemotherapy combined with immunotherapy, we downloaded the transcriptomic dataset GSE207422 (24 samples) from the GEO database (http://www.ncbi.nlm.nih.gov/geo/) consisting of pretreatment samples from patients receiving neoadjuvant chemoimmunotherapy. All clinical information, treatment regimens, and outcomes were obtained from the corresponding publications [22]. All patients received 2–4 cycles of PD-1 antibody plus platinum-based chemotherapy. Among them, 9 patients achieved a major pathological response (MPR), while 15 showed a nonmajor pathological response (NMPR).

Additionally, to explore the ability of gene signatures in predicting immunotherapy efficacy and prognosis, we downloaded NSCLC datasets of patients treated with ICIs monotherapy from the GEO database, including GSE135222 (27 samples) and GSE126044 (16 samples). We used the ComBat function from the sva R package to remove batch effects [23], as the treatment methods and study endpoints in the two datasets were consistent, combining them into a larger Immune Monotherapy Cohort for further analysis, referred to as Immune Monotherapy Cohort in the following text. Of these, 13 patients acquired durable clinical benefit (DCB, responder) while 30 patients acquired nondurable benefit (NDB, nonresponder).

To explore the potential mechanisms underlying gene signature-based predictions of immunotherapy, the transcriptomic and clinical data of NSCLC patients from TCGA-LUAD and TCGA-LUSC were downloaded from the Genome Data Commons (GDC) data portal (https://portal.gdc.cancer.gov), forming the TCGA-NSCLC cohort (929 samples).

2.2 | Clinical Sample Collection at Our Institution

To validate our results, we retrospectively collected formalin-fixed paraffin-embedded (FFPE) tissue samples from 53 early-stage NSCLC patients who received 2–6 cycles of neoadjuvant chemoimmunotherapy at Daping Hospital, China, between August 2017 and June 2024. Primary tumor samples from the lungs and lymph nodes were staged according to the 8th edition of the American Joint Committee on Cancer (AJCC) TNM staging system. Tumor response was assessed using the Response Evaluation Criteria in Solid Tumors version 1.1 (RECIST 1.1). Tumors with 0% viable cells were classified as having a pathological complete response (pCR), and those with $\leq$10% viable cells were classified as having a major pathological response (MPR) [24]. The clinical characteristics, radiologic responses,

TABLE 1 | Clinical characteristics of 53 NSCLC patients.

Characteristics	ALL ($n=53$)	ATF3 high ($n=30$)	ATF3 low ($n=23$)	p
Age [mean (SD)]	61.6 (7.6)	60.8 (8.6)	62.6 (6.0)	0.405
Sex (%)				
Female	6 (11.3)	4 (13.3)	2 (8.7)	0.928
Male	47 (88.7)	26 (86.7)	21 (91.3)	
Smoking (%)				
Never	11 (20.8)	6 (20.0)	5 (21.7)	1
Former or current	42 (79.2)	24 (80.0)	18 (78.3)	
Pathology (%)				
Adeno	15 (28.3)	7 (23.3)	8 (34.8)	0.542
Squamous	38 (71.7)	23 (76.7)	15 (65.2)	
Stage (%)				
I	4 (7.5)	3 (10.0)	1 (4.3)	0.682
II	12 (22.6)	6 (20.0)	6 (26.1)	
III	37 (69.8)	21 (70.0)	16 (69.6)	
Treatment cycles (%)				
≤ 2	31 (58.5)	20 (66.7)	11 (47.8)	0.272
>2	22 (41.5)	10 (33.3)	12 (52.2)	
PD1 antibody (%)				
Nivolumab	4 (7.5)	3 (10.0)	1 (4.3)	0.095
Pembrolizumab	6 (11.3)	1 (3.3)	5 (21.7)	
Tislelizumab	43 (81.1)	26 (86.7)	17 (73.9)	
Chemotherapy (%)				
Docetaxel+platinum drug	3 (5.7)	1 (3.3)	2 (8.7)	0.501
Paclitaxel+platinum drug	35 (66.0)	22 (73.3)	13 (56.5)	
Pemetrexed+platinum drug	15 (28.3)	7 (23.3)	8 (34.7)	
BOR (%)				
CR	2 (3.8)	1 (3.3)	1 (4.3)	0.296
PR	40 (75.5)	25 (83.3)	15 (65.2)	
SD	11 (20.8)	4 (13.3)	7 (30.4)	

Abbreviations: BOR, best overall response; PD, progressive disease; PR, partial response; SD, stable disease.

treatment regimens, and outcome data of the patients are summarized in Table 1.

2.3 | Differential Gene Expression Analysis

RNA-seq data were normalized using the "limma" package in R software. Differentially expressed genes (DEGs) were identified through the application of the DESeq2 package [25]. Genes exhibiting an adjusted p-value of less than 0.05 and an absolute log2 fold change (FC) greater than 2 between MPR and NMPR patient groups were classified as DEGs.

2.4 | Functional Enrichment Analysis

Gene Set Enrichment Analysis (GSEA) [26], a widely used algorithm to identify statistically enriched pathways in ranked gene lists, was conducted using the R package clusterProfiler [27]. The normalized enrichment score (NES) was employed to evaluate the extent of gene set enrichment. In this investigation, a positive NES signifies that the gene set is enriched in MPR/DCB patients, whereas a negative NES denotes enrichment in NMPR/NDB patients. The gene set utilized for functional enrichment analysis was sourced from the Molecular Signature Database (MSigDB, www.broadinstitute.org/msigdb) [28].

2.5 | Immune Infiltration Analysis

CIBERSORT is a widely used tool for deconvolution of the expression matrix of immune cells based on linear support vector regression that quantifies the proportion of infiltrating immune cells by marker gene expression [29]. In our study, we used CIBERSORT to combine the expression of marker genes from 22 immune cells with transcriptomic data from all TCGA-NSCLC patients to determine values for the distribution of tumor-infiltrating lymphocytes. The ESTIMATE R software package uses gene expression profiles to predict stromal and immune cell scores and is also used to calculate the number of these two cell types that allowed us to analyze TCGA-NSCLC purity [30]. In addition, in this study, xCell was used to estimate the abundance of immune cell infiltration in different populations [31].

2.6 | Immunotherapy Response Prediction and Validation

The tumor immune dysfunction and exclusion (TIDE) algorithm is an efficacy prediction tool developed based on TIDE characteristics, which has been validated to efficiently predict therapeutic response to anti-PD-1/CTLA-4 ICIs in melanoma patients [32]. In this study, the TIDE score, T-cell dysfunction score, and T-cell rejection score of TCGA-NSCLC were downloaded from the TIDE Database (http://tide.dfci.harvard.edu/). Patients with a TIDE score >0 were categorized as immunotherapy nonresponders according to established thresholds, whereas patients with a score <0 were defined as potential responders. The immunophenotype score (IPS) has been shown to be a good predictor of immunotherapy sensitivity and measures overall tumor immunogenicity, with higher IPS scores indicating greater sensitivity to immunotherapy [33]. The IPS scores of TCGA NSCLC patients were obtained from TheCancerImmumome Atlas database (TCIA, https://tcia.at/).

2.7 | Immunohistochemistry (IHC)

The expression of ATF3 and PD-L1 proteins in tumor tissues collected at baseline was assessed through a standardized IHC protocol. Slides were deparaffinized, rehydrated, and antigen retrieved, followed by staining with either the ATF3 antibody (catalog no. HPA001562) or the PD-L1 antibody (catalog no. PTM-5075). The bound HRP antibody was detected using the DAB solution (Cat# DA1010, Solarbio Life Science). Slides were counterstained with hematoxylin and bluing reagent. The quantification of ATF3 protein expression was performed by analyzing staining intensity (0–3) and tumor cell area percentage (0%–100%) to calculate an IHC score (0%–300%). Scores below 150% indicated low expression, while scores above 150% indicated high expression, as previously defined [34]. The PD-L1 protein expression level was categorized according to the tumor proportion score (TPS, the percentage of tumor cells with membranous PD-L1 staining). A TPS score of $\geq 50\%$ indicated a high expression group, while $<50\%$ indicated a low expression group. All the immunostaining results were examined and assessed independently on the collected patient samples by two pathologists who were blinded to the clinical characteristics and clinical outcomes of the patients.

2.8 | Statistical Analysis

Statistical analyses were performed using R software (version 4.4.0). Associations between clinicopathological data and molecular characteristics were examined using the χ^2 test for categorical variables, while the Wilcoxon rank-sum test was used for continuous variables exhibiting nonparametric distributions. Survival analyses for progression-free survival (PFS) and disease-free survival (DFS) were performed using Kaplan–Meier estimation combined with the log-rank test. The predictive value of quantitative indicators of candidate gene expression was assessed using subject ROC curves, and the area under the ROC curve (AUC) was used as an indicator for comparing the strengths and weaknesses of the models. p-values of <0.05 were considered to be statistically significant ($^*p<0.05$; $^{**}p<0.01$; $^{***}p<0.001$; $^{****}p<0.0001$).

3 | Results

3.1 | Molecular Characteristics of NSCLC Patients Pathologically Responding to Neoadjuvant Chemoimmunotherapy

We obtained a dataset of pretreatment samples of NSCLC patients receiving neoadjuvant chemoimmunotherapy from the GEO database (GSE207422). Patient demographics and disease characteristics were equally distributed across response groups (Table S1). By comparing gene expression between patients who achieved major pathological response (MPR, $n=9$) and those who did not (NMPR, $n=15$), 510 genes were found to be significantly upregulated and 236 genes downregulated in the MPR group(false discovery rate [FDR] ≤ 0.05, Benjamini-Hochberg [BH] correction) (Figure 1A,B). Additionally, we used CIBERSORT to explore the tumor immune landscape. Among the 22 types of immune cells analyzed, the only significant difference was an increased abundance of $CD8^+$ T cells (Figure 1C).

GSEA revealed significant upregulation (FDR <0.05) in the MPR tumor group, which were involved in the Allograft rejection, interferon alpha and gamma response, and complement gene sets, while the NMPR tumor group was primarily enriched in the MYC targets, G2M checkpoint, E2F targets, and epithelial mesenchymal-transition gene sets (Figure 1D). Previous studies suggest the interferon response pathway is crucial among enriched pathways [35–39]. Thus, we examined its potential in predicting immunotherapy efficacy using ROC curves. The analysis revealed similar predictive performance for the interferon alpha and gamma response pathways, with AUC values of 0.807 and 0.8, respectively (Figure S1A,B). In addition, the combination of interferon alpha and gamma response pathways (interferon-responsive pathway) also predicted the efficacy of neoadjuvant immunotherapy with an AUC value of 0.822 (Figure 1E). In another independent NSCLC immune monotherapy cohort (Immune Monotherapy Cohort), GSEA analysis showed a significant enrichment of the interferon response pathway in responders (Figure 1F), and ROC analysis demonstrated that this pathway was effective in predicting the response to ICIs therapy (Figure 1G). In conclusion, the enrichment of the interferon response pathway was closely related to the response to immunotherapy.

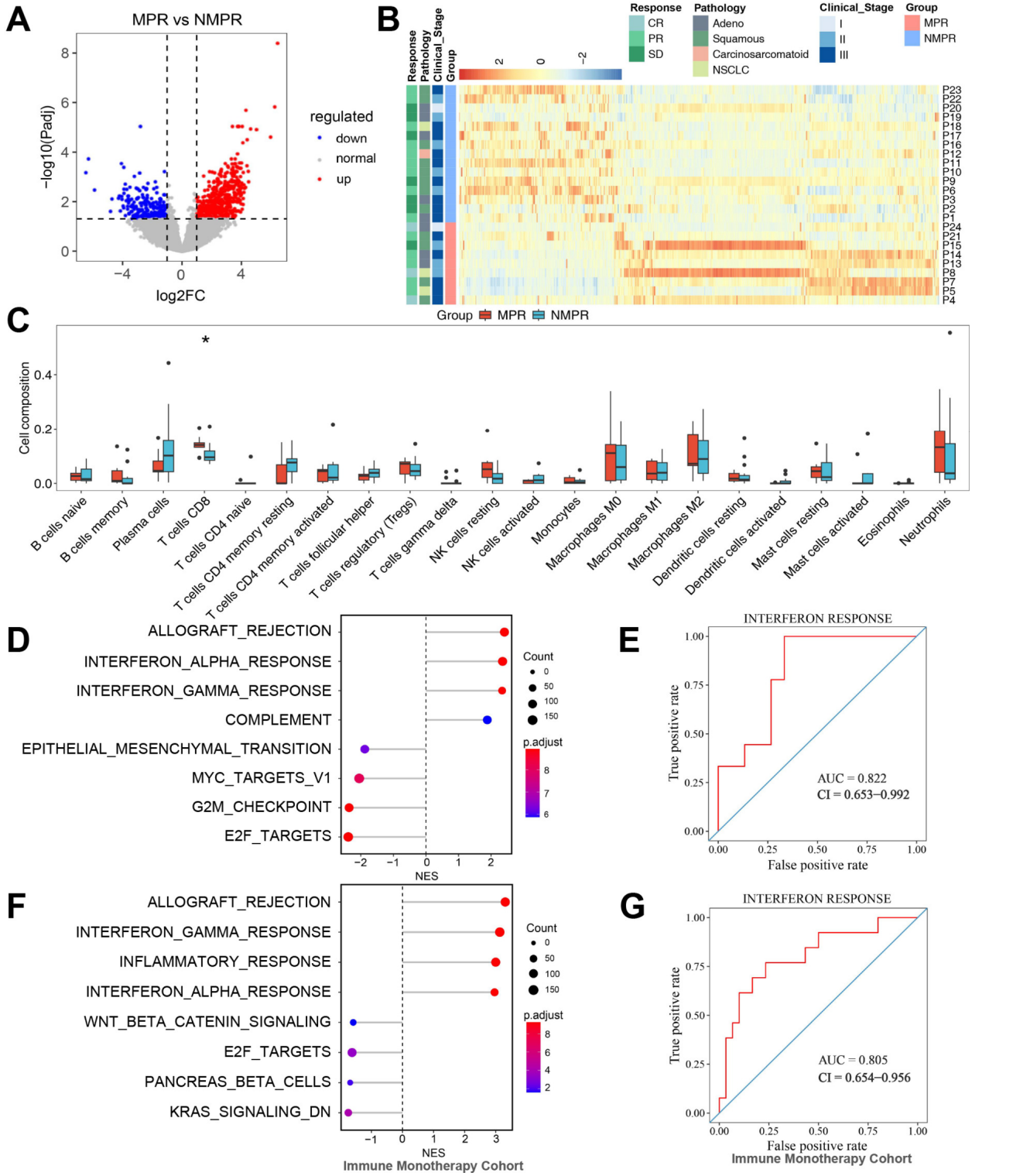

FIGURE 1 | Pretreatment tumor characteristics associated with differing efficacy of immunotherapy combined with chemotherapy. (A) Volcano plot showing differentially expressed genes in MPR ($n = 9$) compared with NMPR ($n = 15$). Red and blue dots represent the significantly upregulated and downregulated genes, respectively. (B) Heatmap of pretreatment differentially expressed genes between MPR ($n = 9$) and NMPR ($n = 15$). (C) The enrichment of tumor-infiltrating immune cells as determined by cibersort deconvolution. MPR ($n = 9$); NMPR ($n = 15$). (D) Bubble chart shows the results of gene set enrichment. MPR ($n = 9$) to NMPR ($n = 15$) tumor groups, with MPR as reference. NES, normalized enrichment score. (E) ROC curve is shown for INFERON RESPONSE pathway (Consisting of HALLMARK_INTERFERON_ALPHA_RESPONSE and HALLMARK_INTERFERON_GAMMA_RESPONSE). AUC, area under the curve. (F) Bubble chart shows the results of gene set enrichment in the Immune Monotherapy Cohort. DCB ($n = 13$) to NDB ($n = 30$) tumor groups, with DCB as a reference. (G) ROC curve is shown for INTERFERON RESPONSE pathway in the Immune Monotherapy Cohort. AUC refers to the area under the curve. *$p < 0.05$; **$p < 0.01$; ***$p < 0.001$; ****$p < 0.0001$.

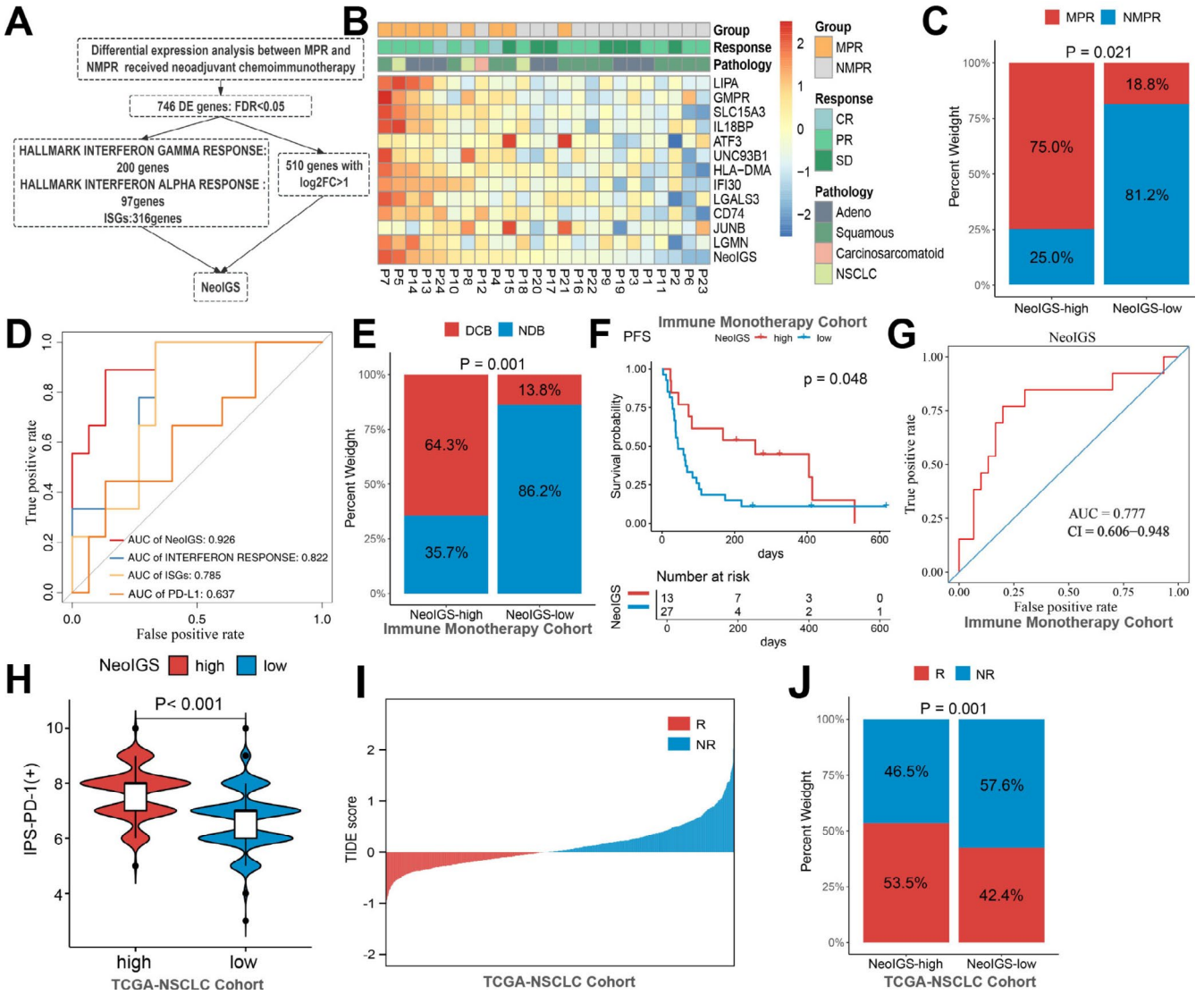

FIGURE 2 | Generate and validate expression signatures associated with MPR. (A) Flowchart illustrating the generation of the NeoIGS signature. (B) Heatmap of genes incorporated in the NeoIGS signature. (C) Histogram shows the cumulative distribution of chmoimmunotherapy response in patients in the NeoIGS-high group and NeoIGS-high group. (D) Predictive abilities of NeoIGS signature, INFERON RESPONSE signature, ISGs signature, and PD-L1 expression are compared by ROC curves. (E–G) NeoIGS was validated in the Immune Monotherapy Cohort. Cumulative distribution bar charts of the immunotherapy response in the NeoIGS-high ($n = 14$) and NeoIGS-low ($n = 29$) groups (E), PFS curves (F), and ROC curves (G) are shown. *p*-values for the KM analysis are derived from the log-rank test, while *p*-values in the bar charts represent Fisher's exact test. (H) Violin plot shows the relationship between the NeoIGS score and IPS scores. (I) Waterfall plot of TIDE prediction scores for the TCGA-NSCLC cohort, with red and blue representing responders and nonresponders, respectively. (J) Histogram showing the cumulative distribution of TIDE-predicted immunotherapy responses in the NeoIGS-high group versus the NeoIGS-low group.

3.2 | A Novel 12-Gene Signature Can Accurately Predict the Response to ICB Combined With Chemotherapy in Nonsmall-Cell Lung Cancer

Based on the potential value of the interferon signaling pathway in predicting the efficacy of chemoimmunotherapy, we sought to screen for key proteins with positive predictive effects. To this end, we collected three sets of interferon-related genes "HALLMARK-INTERFERON-GAMMA-RESPONSE", "HALLMARK-INTERFERON-ALPHA-RESPONSE," and ISG [40], and by intersecting them with genes significantly upregulated in patients with MPR, a subset of the interferon signaling pathway, NeoIGS, was obtained (Figure 2A). This subset consisted of 12 genes: "LIPA, GMPR, SLC15A3, IL18BP, UNC93B1, HLA-DMA, IFI30, LGALS3, CD74, JUNB, LGMN, and ATF3" (Figure 2B).

We evaluated NeoIGS expression in each sample using ssGSEA, defining the NeoIGS high group as patients within the third tertile and classifying the remaining patients as the NeoIGS low group [41]. A significantly higher proportion of patients with high NeoIGS ($n = 8$) achieved MPR compared to those with low NeoIGS ($n = 16$) (75.0% vs. 18.8%, $p = 0.021$, Figure 2C). ROC analysis showed that NeoIGS was the most effective genetic signature for distinguishing patients with MPR from those with NMPR, with an AUC of 0.926 (Figure 2D). In addition, in the immune monotherapy cohort (Immune Monotherapy Cohort), there were more responders in the high NeoIGS ($n = 14$) group

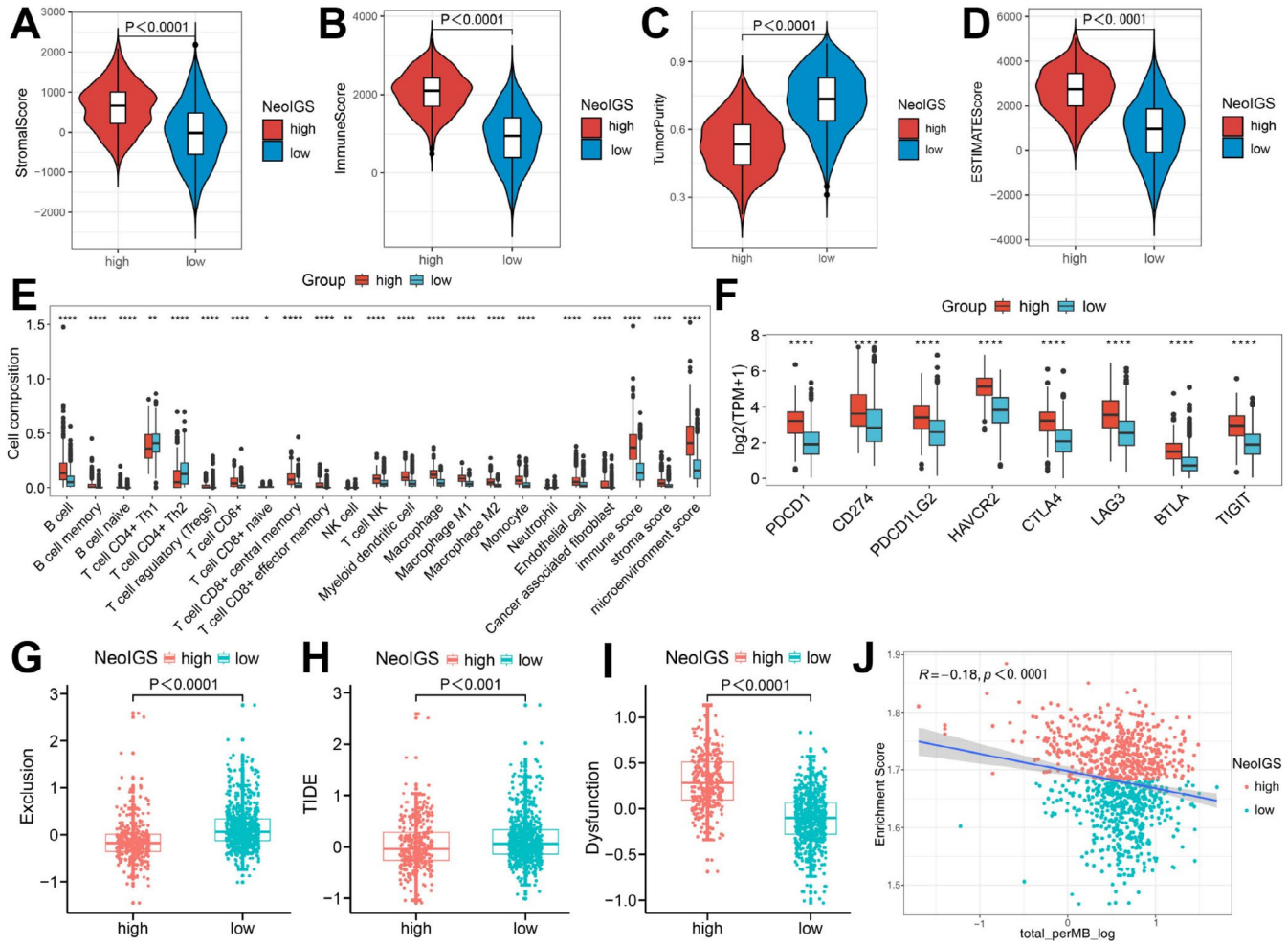

FIGURE 3 | The intrinsic relationship between the NeoIGS signature and immunotherapy response. (A–D) The box plots show lower tumor purity (A) and higher stromal scores (B), immune scores (C), and ESTIMATE scores (D) in the NeoIGS-high group. (E) The proportion of tumor-infiltrating immune cells in the NeoIGS-high group versus the NeoIGS-low group was measured using xCell. (F) The box plots display the different expression levels of typical immune inhibitory receptors(PDCD1, CTLA4, LAG3, BTLA, CD274, HAVCR2, VSIR, and PDCD1LG2) between the two groups. (G–I) The box plots display the TIDE scores (G), exclusion scores (H), and dysfunction scores (I) for the NeoIGS-high group and the NeoIGS-low group, respectively. (J) Scatter plot shows the correlation between NeoIGS and TMB. *$p<0.05$; **$p<0.01$; ***$p<0.001$; ****$p<0.0001$.

than in the low NeoIGS ($n=29$) group (64.3% vs. 13.8%, $p=0.001$, Figure 2E). High NeoIGS was associated with longer mPFS (8.6 vs. 1.5 months, $p=0.048$, Figure 2F), and ROC curve analysis showed that NeoIGS also predicted the efficacy of monotherapy with ICIs (AUC = 0.777, Figure 2G).

Additionally, we explored the correlation between NeoIGS and IPS [33] as well as TIDE [32] scores to validate the predictive potential of NeoIGS in ICIs treatment. IPS and TIDE scores are recognized predictors of immunotherapy, and we conducted the analysis using the TCGA-NSCLC cohort. A higher IPS score is generally associated with improved efficacy of ICIs therapy, and our results demonstrated that the high NeoIGS expression group exhibited higher IPS scores (Figure 2H). We next used TIDE to predict the population that could benefit from immunotherapy and found that a higher proportion of patients with high NeoIGS scores benefited from treatment (53.3% vs. 39.0%, $p<0.001$, Figure 2I). In summary, the NeoIGS signature can identify responders to ICIs therapy in NSCLC and is associated with longer PFS.

3.3 | The NeoIGS Gene Signature Captures a Unique Immune Microenvironment

The pattern of immune infiltration in the tumor microenvironment plays a key role in the efficacy of immunotherapy. We performed the following explorations using the TCGA-NSCLC cohort. First, the ESTIMATE function was used to assess the proportion of stromal and immune cells infiltrated within the tumor and to infer tumor purity. The results showed that the NeoIGS-high group had higher immune, stromal, and ESTIMATE scores but lower tumor purity compared to the NeoIGS-low group (Figure 3A–D). In parallel, we used xCell to assess the relative abundance of tumor-infiltrating immune cell populations. The analysis showed that almost all immune cell types were significantly more abundant in the NeoIGS-high group (Figure 3E), which is consistent with the results of the ESTIMATE assessment. Next, we analyzed the expression profiles of typical immune checkpoint molecules (PD-1, CD274, PDCD1LG2, HAVCR2, CTLA4, LAG3, BTLA, and TIGIT) in the two groups and found that the levels of immune checkpoint

molecules were significantly upregulated in the NeoIGS-high group (Figure 3F).

In addition, we calculated TIDE scores for both groups to assess the potential of tumor immune evasion. A lower TIDE score was associated with a higher likelihood of immunotherapy benefit. The results showed that the TIDE score was significantly lower in the NeoIGS-high group compared to the NeoIGS-low group (Figure 3G–I). Meanwhile, we explored the correlation between NeoIGS score and TMB, and the results showed a weak correlation between the two (Figure 3J), suggesting that NeoIGS score may be a predictor of immunotherapy efficacy independent of TMB.

In conclusion, these findings suggest that tumors with high NeoIGS scores exhibit increased immune cell infiltration and upregulation of immune checkpoint-associated molecules, indicating greater sensitivity to immune checkpoint therapy.

3.4 | ATF3 Can Predict the Pathological Response to Neoadjuvant Chemoimmunotherapy

In search of a more economical and efficient detection indicator, this study evaluated the correlation between 12 NeoIGS genes and pathological responses by ROC curves. The results showed that ATF3 exhibited the optimal predictive efficacy (AUC = 0.911, Figure 4A). Specifically, the expression level of ATF3 was significantly higher in the MPR group compared to the NMPR group (Figure 4B). Further analysis revealed that the proportion of patients achieving MPR was significantly higher in the ATF3 high-expression group ($n = 8$) than in the ATF3 low-expression group ($n = 16$) (87.5% vs. 12.5%, $p < 0.01$, Figure 4C). Additionally, we analyzed PD-L1, a clinically commonly used predictive biomarker, and found no significant difference in PD-L1 expression levels between the MPR and NMPR groups (Figure 4D). Similarly, there was no significant difference in the MPR rate between the PD-L1 high-expression group and the PD-L1 low-expression group (Figure 4E). The above results suggest that, compared to PD-L1, the transcriptional level of ATF3 in the tumor prior to treatment appears to be a better predictor of the beneficiaries of neoadjuvant chemoimmunotherapy in NSCLC patients.

Subsequently, we further explored the correlation between ATF3 and the efficacy of monotherapy in an independent dataset of patients receiving ICIs (the Immune Monotherapy Cohort). The results showed that Irrespective of the level of ATF3 expression, no statistically significant difference was observed in the proportion of patients experiencing DCB (Figure 4F). Survival analysis showed no statistically significant difference in PFS between the two groups (Figure 4G). This indicates that ATF3 exhibits limited predictive value for immune monotherapy efficacy.

In addition, we used CIBERSORT to assess the immune cell populations in the TCGA-NSCLC cohort. the ATF3-high group had more follicular helper T cells and resting NK cells, but fewer regulatory T cells and resting mast cells (Figure 4H). The presence of Tregs in the microenvironment may be one of the key factors that ultimately lead to drug resistance. Overall, these findings suggest that ATF3 expression is strongly associated with the effectiveness of neoadjuvant chemoimmunotherapy.

3.5 | Predictive Value of ATF3 Protein Expression

To further validate the findings from the transcriptome data, we recruited 53 NSCLC patients who received neoadjuvant chemoimmunotherapy and prospectively collected pretreatment biopsy samples from these patients. This cohort included 6 females (11.3%) and 47 males (88.7%), with an average age of 61.6 years (range: 46–77 years). Squamous cell carcinoma (38/53, 71.7%) was the most common histological type, followed by adenocarcinoma (15/53, 28.3%). All patients were at stages I–III. All patients received ICIs combined with platinum-based doublet chemotherapy. The majority received the tislelizumab (43/53, 81.1%), while others received nivolumab (4/53, 7.5%) and pembrolizumab (6/53, 11.3%). A swimmer plot summarized the treatment details of the 53 NSCLC patients (Figure 5A). After 2–6 cycles of neoadjuvant chemoimmunotherapy, the radiographic ORR (PR plus CR) was79.2% (42/53). The pathological response of the 53 patients was then assessed by two independent and well-trained pathologists, with 64% (34/53) and 36% (19/53) of patients achieving MPR/pCR and NMPR, respectively (Figure 5B,C).

We quantified the expression of ATF3 in each sample using immunohistochemistry (IHC). Among them, 56.6% of the cases (30/53) exhibited high expression of ATF3 (IHC score ≥ 150). Representative microscopic images of ATF3 IHC staining are shown in Figure 6A. The ATF3-high and ATF3-low groups were comparable in terms of gender, age, smoking status, tumor stage, and treatment cycles (Table 1). Statistical analysis revealed that the MPR rate of all patients was 64.2%, and the pCR and MPR rate in the ATF3-high group was significantly higher than that in the ATF3-low group (pCR: 66.7% vs. 21.7%, $p = 0.003$; MPR rate: 90.0% vs. 30.4%, $p < 0.001$, Figure 6B,C). The ATF3 IHC score in the MPR group was significantly higher than that in the NMPR group (204.3 vs. 23.0, $p < 0.001$, Figure 6D). The cohort had a median follow-up duration of 13.6 months (range: 1.7–63.2 months). Within the ATF3-high expression group, the hazard ratio (HR) for tumor recurrence was calculated to be 0.23 (95% CI: 0.07–0.76), and patients with elevated ATF3 expression experienced a significantly prolonged DFS ($p = 0.041$). The 12-month DFS rate was 100.0% in the ATF3-high group, compared to 71.8% (95% CI: 54.9%–93.8%) in the ATF3-low group. Similarly, the 24-month DFS rate was higher in the ATF3-high group than in the ATF3-low group (78.7% vs. 55.2%) (Figure 6E).

In addition, this study analyzed the correlation between PD-L1 expression and pathological response. The results showed that there was no significant difference in the pCR and MPR rate between the PD-L1 high-expression group (TPS ≥ 50%) and the low-expression group (TPS < 50%) (pCR: 56.5% vs. 40.0%, $p = 0.359$; MPR rate: 69.6% vs. 60.0%, $p = 0.667$), and there was also no statistically significant difference in the DFS between the two groups (Figure 6F–J). This reconfirmed the limited predictive value of PD-L1 in immunocombination chemotherapy treatment. In conclusion, consistent with the transcriptomic data, ATF3 protein levels were effective in predicting the

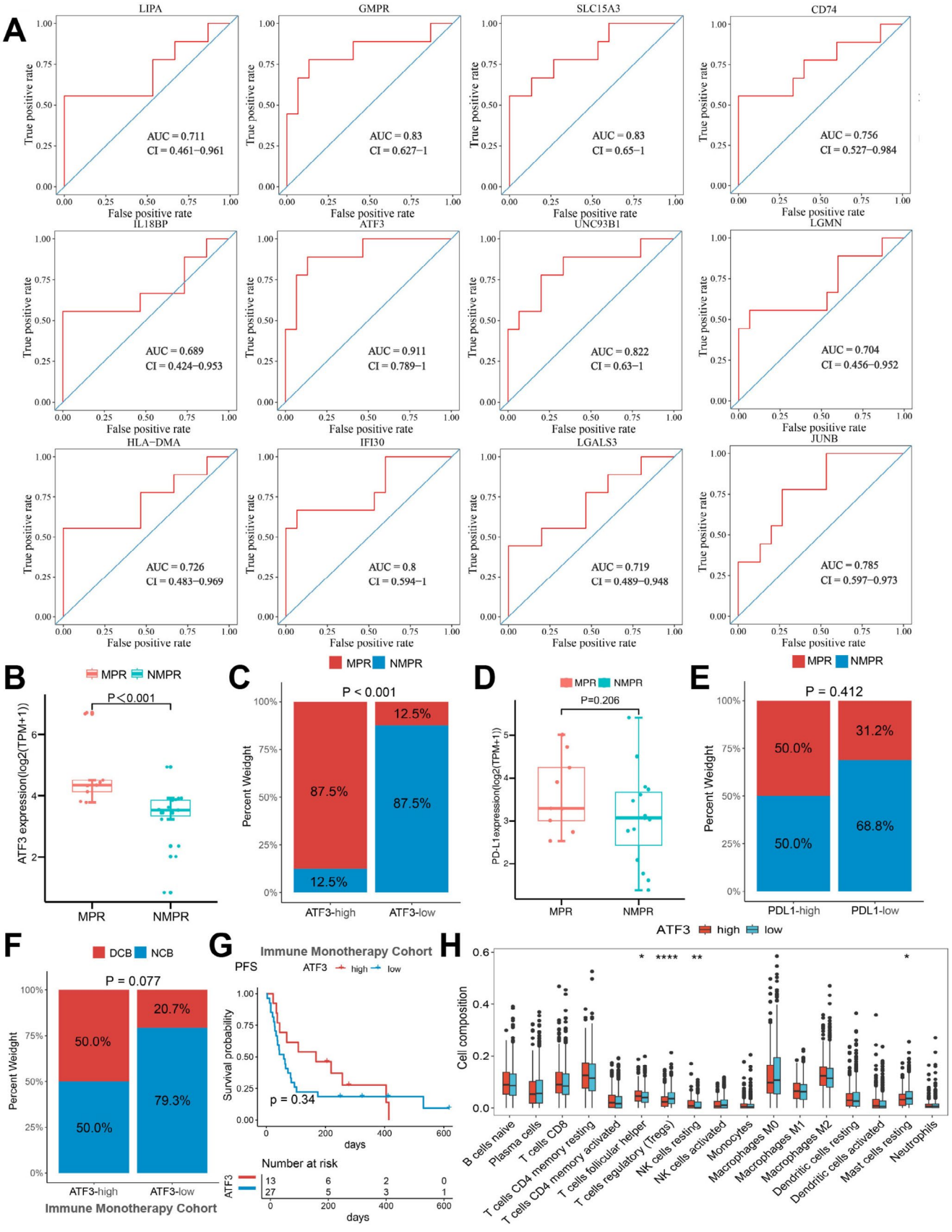

FIGURE 4 | Legend on next page.

FIGURE 4 | The screening of ATF3 as the optimal predictor of therapeutic efficacy. (A) The ROC curve analyzed the predictive role of the 12 genes comprising the NeoIGS signature for the pathological response to neoadjuvant chemoimmunotherapy. (B) The mRNA expression levels of ATF3 in the MPR ($n = 9$) and NMPR ($n = 15$) groups. (C) The histogram shows the cumulative distribution of pathological responses to neoadjuvant chemoimmunotherapy in patients from the ATF3-high and ATF3-low groups. (D) The mRNA expression levels of PD-L1 in the MPR and NMPR groups. (E) The histogram shows the cumulative distribution of pathological responses to neoadjuvant chemoimmunotherapy in patients from the PD-L1-high and PD-L1-low groups. (F) The histogram shows the cumulative distribution of immunotherapy responders in patients from the Immune Monotherapy Cohort, comparing the ATF3-high group with the ATF3-low group. (G) PFS curves of patients with high and low expression of ATF3 in the Immune Monotherapy Cohort. (H) Using CIBERSORT deconvolution to measure the proportion of tumor-infiltrating immune cells in the ATF3-high and ATF3-low groups. *$p < 0.05$; **$p < 0.01$; ***$p < 0.001$; ****$p < 0.0001$.

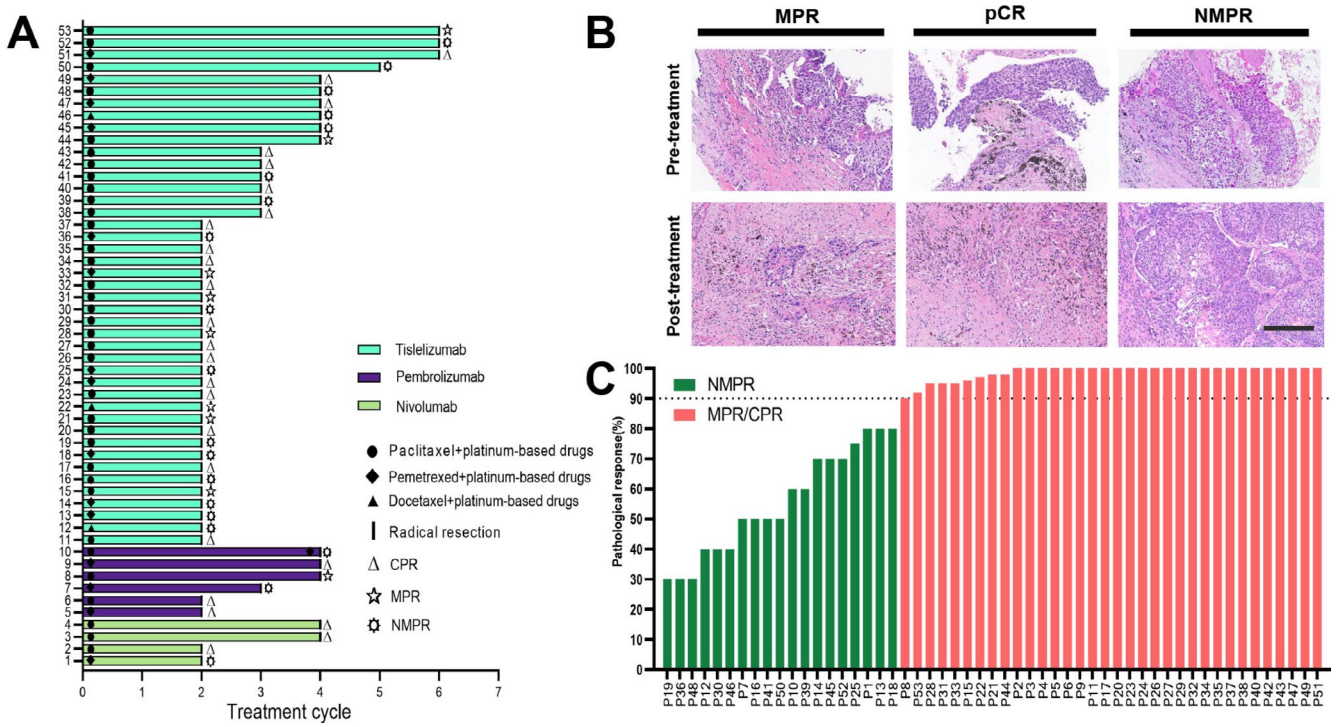

FIGURE 5 | Information on anti-PD-1 treatment combined with chemotherapy in the clinical cohort. (A) Swimmer plot demonstrates the treatment regimen and pathological response of 53 NSCLC patients. (B) Pathological evaluation of 53 NSCLC patients receiving chemotherapy plus anti-PD-1 therapy. (C) Representative histological results (H&E staining) of the pretreatment tumor biopsy and surgically resected tissue from patients having MPR (left), pCR (middle), and NMPR (right). Scale bar: 100 μm.

pathological response and survival benefit of NSCLC patients to neoadjuvant chemoimmunotherapy.

4 | Discussion

ICIs have significantly improved clinical outcomes in NSCLC and have become one of the most effective first-line cancer treatments [42]. However, traditional predictive biomarkers for ICI monotherapy, such as PD-L1 expression and TMB, have limitations in predicting the efficacy of chemoimmunotherapy [15–18]. There is increasing evidence of a significant correlation between pathological response and patient prognosis [20, 21, 43]. With the increasing use of chemoimmunotherapy in the clinic, reliable predictive biomarkers are needed to accurately assess treatment efficacy, especially pathological response.

We retrospectively analyzed transcriptomic data from pre-treatment biopsies of patients undergoing neoadjuvant chemoimmunotherapy. We discovered that the enrichment of pathways related to allograft rejection, IFN responses, and complement genes correlates with a higher chance of achieving MPR post-treatment. Multiple studies have demonstrated that active IFN signaling in the tumor microenvironment is a critical mediator and a positive predictor of tumor response to ICIs [35–39]. Consequently, the present study focused on assessing the predictive significance of the IFN signaling pathway in chemoimmunotherapy.

Additionally, different components of the IFN signaling pathway have been associated with ICIs responsiveness or resistance mechanisms [44]. However, current studies have not yet elucidated which key proteins in the IFN signaling pathway are effective in predicting the efficacy of chemoimmunotherapy, particularly the degree of pathological remission with neoadjuvant therapy. In this study, we identified a subset of genes within the IFN signaling pathway, termed NeoIGS, by cross-analysis of differentially upregulated genes in MPR patients. NeoIGS

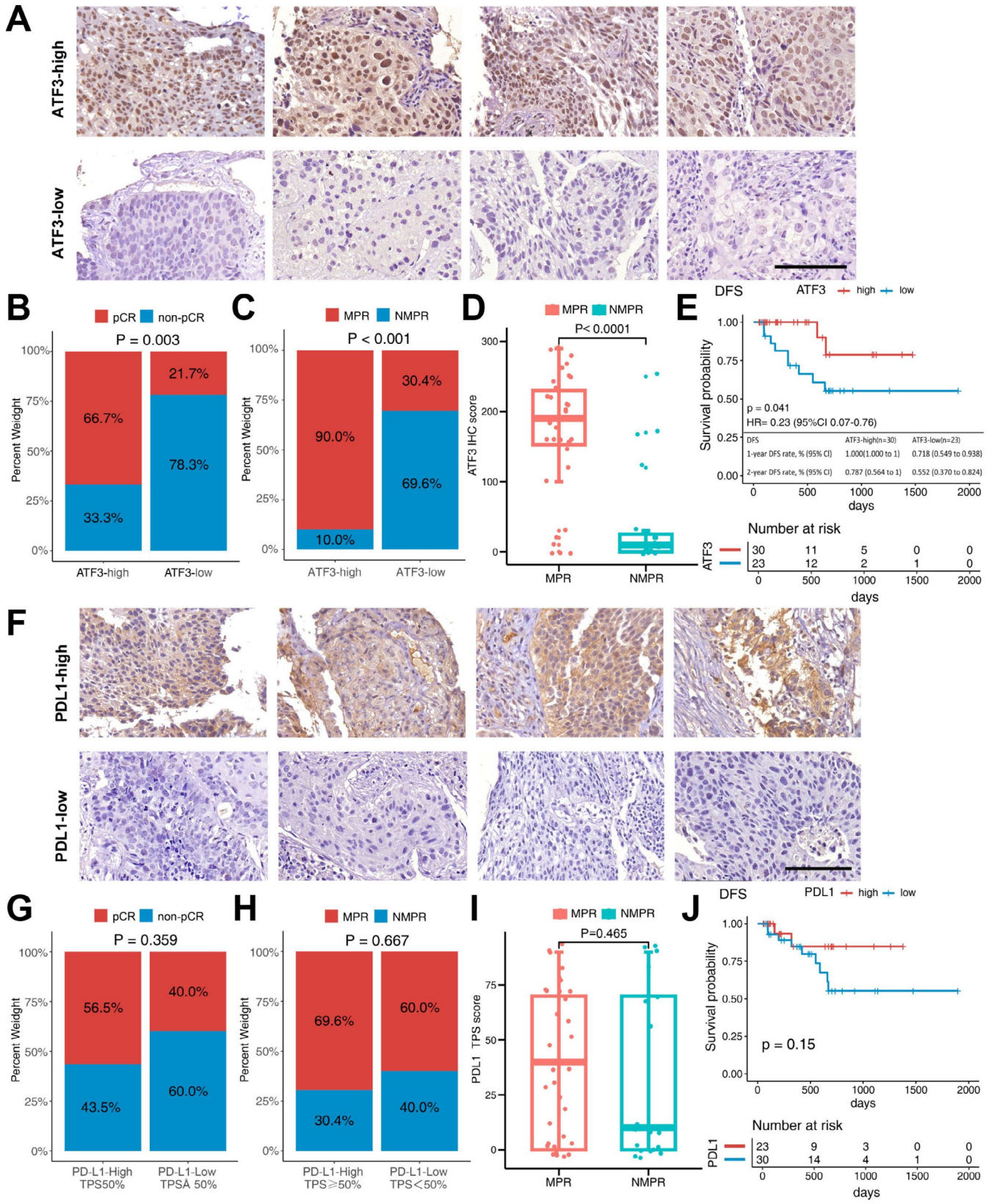

FIGURE 6 | Validation in 53 clinical samples using IHC. (A) representative staining image of the ATF3-high ($n = 30$) and ATF3-low ($n = 23$) groups. Scale bar: 100 μm. (B, C) The histogram demonstrates the differences in pCR and MPR rates between the ATF3-high group and the ATF3-low group. (D) The IHC scores of ATF3 in the MPR and NMPR groups. (E) DFS curves of patients with high and low protein expression of ATF3. (F) The representative staining images of the PD-L1-high ($n = 23$) and PD-L1-low ($n = 30$) groups. Scale bar: 100 μm. (G, H) The histogram demonstrates the differences in pCR and MPR rates between the PD-L1-high group and the PD-L1-low group. (I) The TPS scores of PD-L1 in the MPR and NMPR groups. (J) DFS curves of patients with high and low protein expression of PD-L1.

effectively predicts the pathological response of NSCLC patients to neoadjuvant chemoimmunotherapy, outperforming the IFN signaling pathway itself and PD-L1. It also forecasts the efficacy and prognosis of NSCLC patients receiving ICI monotherapy. Both IPS [33] and TIDE [32] scores, validated as predictors of immunotherapy efficacy, showed that patients with higher NeoIGS scores had higher IPS scores and lower TIDE scores, indicating that these patients are more likely to benefit from immunotherapy. Additionally, ESTIMATE and Xcell analyses suggest that NeoIGS scores capture patients with immune cell infiltration. Ongoing interactions between tumor cells and the tumor microenvironment drive tumorigenesis, progression, and response to therapy [45, 46]. In addition, tumor-infiltrating lymphocytes and their spatial distribution can predict pathological responses to neoadjuvant immunotherapy [47]. Taken together, these findings suggest that NeoIGS may serve as a promising biomarker for immunotherapy in NSCLC patients.

Although many studies have attempted to identify beneficiaries of immunotherapies through gene combinations, high testing costs, lack of standardized protocols, and regulatory and ethical challenges have prevented their widespread adoption in clinical practice. Therefore, we identified the clinically applicable biomarker for chemoimmunotherapy, ATF3, an adaptive response gene involved in cellular adaptation to external and internal environmental changes such as DNA damage, cellular injury, and oxidative stress [48], by ROC curve analysis. Recent studies have shown that ATF3 plays a key role in immunotherapy. For example, Liu et al. reported that inhibition of ADORA1 promotes ATF3 binding to the PD-L1 promoter, thereby increasing PD-L1 expression and facilitating immune escape [49]. Another study found that tumor RGS1 affects $CD8^+$ T cell infiltration and antigen processing by activating STAT1 and inducing IFN-γ-stimulated genes via the ATF3-IFNGR1 axis [50]. Our study showed that ATF3 appeared to regulate immune cell infiltration, with lower Treg cell infiltration observed in the high-expressing ATF3 group. Previous studies have shown that lower intratumoral Treg/$CD8^+$ T-cell ratios are strongly associated with better immunotherapy outcomes [51]. Taken together, ATF3 may facilitate chemoimmunotherapy by regulating PD-L1 expression and modulating immune cell infiltration.

This study also evaluated the predictive value of PD-L1 in neoadjuvant chemoimmunotherapy. The results showed that no significant correlation was observed between PD-L1 expression levels and pathological remission in either transcriptomic data or clinical samples, which further supports the limitations of PD-L1 as a predictive biomarker in chemoimmunotherapy and suggests the need to develop more effective biomarkers to screen for the beneficiary population of combination therapy. Notably, in the cohort of 53 patients in this study, the MPR rate in the ATF3 high-expression group reached 90.0%. Despite the limited sample size, it still suggests that ATF3 is expected to be a potential biomarker for the efficacy of chemoimmunotherapy. Interestingly, immunohistochemical staining showed that ATF3 was mainly localized in the nucleus of tumor cells, consistent with the results of previous studies [52], and this subcellular localization feature provides feasibility for clinical detection of ATF3 expression.

The present study has the following limitations: first, the small sample size may affect the reliability of the conclusions, and the predictive efficacy of ATF3 on pathological response and prognosis needs to be verified by a multicenter large-sample study. second, ATF3 is mainly applicable to the prediction of chemoimmunotherapy combination therapy, and the predictive efficacy decreases in single-agent therapy, which may be related to its strong correlation with the response to chemotherapy. Previous studies have shown that high ATF3 expression enhances the efficacy of cisplatin in lung [53, 54] and gastric cancer [55] and increases the sensitivity of nasopharyngeal carcinoma cells to paclitaxel [56]. finally, the mechanism of action of ATF3 has not yet been fully elucidated, and its biological function in neoadjuvant chemoimmunotherapy needs to be further explored.

In summary, this study not only reaffirms the predictive value of the IFN pathway, but also innovatively proposes a subset of IFN signals that are closely related to immunotherapy and establishes ATF3 as a potential marker for predicting the efficacy of neoadjuvant chemotherapy immunotherapy.

Author Contributions

Yong He and Chao He conceptualized and designed the study; Chao He, Conghua Lu, and Rui Han performed the development of methodology; Chao He and Daijuan Huang were involved in data acquisition; Chao He and Rui Han performed data analysis and interpretation; Chao He, Yimin Zhang, Rui Han, and Yong He were involved in writing, reviewing, and revising the manuscript; Taiming Zhang, Peng Zhong, and Yuwen Deng provided administrative, technical, and material support; Conghua Lu, Rui Han, and Yong He were involved in study supervision. All authors have read and approved this article.

Acknowledgments

We sincerely thank Prof. Peng Zhang's research groups for providing transcriptomics data in the GEO databases.

Ethics Statement

This study was approved by the Ethics Committees of the Daping Hospital, Army Medical University (No. 2023123). This study conformed to the tenets of the Declaration of Helsinki.

Conflicts of Interest

The authors declare no conflicts of interest.

Data Availability Statement

Bulk transcriptome data (GSE53625, GSE135222, GSE126044) can be obtained from the GEO database (http://www.ncbi.nlm.nih.gov/geo/). Furthermore, gene expression information for TCGA patients was downloaded from The Cancer Genome Atlas (TCGA) database (https://portal.gdc.cancer.gov/). Other data are available upon reasonable request.

References

1. F. Bray, M. Laversanne, H. Sung, et al., "Global Cancer Statistics 2022: GLOBOCAN Estimates of Incidence and Mortality Worldwide for 36 Cancers in 185 Countries," *CA: A Cancer Journal for Clinicians* 74 (2024): 229–263, https://doi.org/10.3322/caac.21834.

2. A. A. Thai, B. J. Solomon, L. V. Sequist, J. F. Gainor, and R. S. Heist, "Lung Cancer," *Lancet* 398 (2021): 535–554, https://doi.org/10.1016/S0140-6736(21)00312-3.

3. F. R. Hirsch, G. V. Scagliotti, J. L. Mulshine, et al., "Lung Cancer: Current Therapies and New Targeted Treatments," *Lancet* 389 (2017): 299–311, https://doi.org/10.1016/S0140-6736(16)30958-8.

4. S. N. Gettinger, L. Horn, L. Gandhi, et al., "Overall Survival and Long-Term Safety of Nivolumab (Anti-Programmed Death 1 Antibody, BMS-936558, ONO-4538) in Patients With Previously Treated Advanced Non-Small-Cell Lung Cancer," *Journal of Clinical Oncology* 33 (2015): 2004–2012, https://doi.org/10.1200/JCO.2014.58.3708.

5. J. R. Brahmer, S. S. Tykodi, L. Q. M. Chow, et al., "Safety and Activity of Anti-PD-L1 Antibody in Patients With Advanced Cancer," *New England Journal of Medicine* 366 (2012): 2455–2465, https://doi.org/10.1056/NEJMoa1200694.

6. D. F. McDermott, C. G. Drake, M. Sznol, et al., "Survival, Durable Response, and Long-Term Safety in Patients With Previously Treated Advanced Renal Cell Carcinoma Receiving Nivolumab," *Journal of Clinical Oncology* 33, no. 18 (2015): 2013–2020, https://doi.org/10.1200/JCO.2014.58.1041.

7. M. Reck, J. Remon, and M. D. Hellmann, "First-Line Immunotherapy for Non-Small-Cell Lung Cancer," *Journal of Clinical Oncology* 40 (2022): 586–597, https://doi.org/10.1200/JCO.21.01497.

8. E. B. Garon, N. A. Rizvi, R. Hui, et al., "Pembrolizumab for the Treatment of Non-Small-Cell Lung Cancer," *New England Journal of Medicine* 372 (2015): 2018–2028, https://doi.org/10.1056/NEJMoa1501824.

9. J. A. Thompson, "New NCCN Guidelines: Recognition and Management of Immunotherapy-Related Toxicity," *Journal of the National Comprehensive Cancer Network* 16 (2018): 594–596, https://doi.org/10.6004/jnccn.2018.0047.

10. T. S. K. Mok, Y.-L. Wu, I. Kudaba, et al., "Pembrolizumab Versus Chemotherapy for Previously Untreated, PD-L1-Expressing, Locally Advanced or Metastatic Non-Small-Cell Lung Cancer (KEYNOTE-042): A Randomised, Open-Label, Controlled, Phase 3 Trial," *Lancet* 393 (2019): 1819–1830, https://doi.org/10.1016/S0140-6736(18)32409-7.

11. A. Sezer, S. Kilickap, M. Gümüş, et al., "Cemiplimab Monotherapy for First-Line Treatment of Advanced Non-Small-Cell Lung Cancer With PD-L1 of at Least 50%: A Multicentre, Open-Label, Global, Phase 3, Randomised, Controlled Trial," *Lancet* 397 (2021): 592–604, https://doi.org/10.1016/S0140-6736(21)00228-2.

12. M. D. Hellmann, T.-E. Ciuleanu, A. Pluzanski, et al., "Nivolumab Plus Ipilimumab in Lung Cancer With a High Tumor Mutational Burden," *New England Journal of Medicine* 378 (2018): 2093–2104, https://doi.org/10.1056/NEJMoa1801946.

13. M. D. Hellmann, L. Paz-Ares, R. Bernabe Caro, et al., "Nivolumab Plus Ipilimumab in Advanced Non-Small-Cell Lung Cancer," *New England Journal of Medicine* 381 (2019): 2020–2031, https://doi.org/10.1056/NEJMoa1910231.

14. N. A. Rizvi, B. C. Cho, N. Reinmuth, et al., "Durvalumab With or Without Tremelimumab vs Standard Chemotherapy in First-Line Treatment of Metastatic Non–Small Cell Lung Cancer: The MYSTIC Phase 3 Randomized Clinical Trial," *JAMA Oncology* 6, no. 5 (2020): 661–674, https://doi.org/10.1001/jamaoncol.2020.0237.

15. Y.-K. Kang, L.-T. Chen, M.-H. Ryu, et al., "Nivolumab Plus Chemotherapy Versus Placebo Plus Chemotherapy in Patients With HER2-Negative, Untreated, Unresectable Advanced or Recurrent Gastric or Gastro-Oesophageal Junction Cancer (ATTRACTION-4): A Randomised, Multicentre, Double-Blind, Placebo-Controlled, Phase 3 Trial," *Lancet Oncology* 23 (2022): 234–247, https://doi.org/10.1016/S1470-2045(21)00692-6.

16. C. Langer, S. Gadgeel, H. Borghaei, et al., "OA04.05 KEYNOTE-021: TMB and Outcomes for Carboplatin and Pemetrexed With or Without Pembrolizumab for Nonsquamous NSCLC," *Journal of Thoracic Oncology* 14 (2019): S216, https://doi.org/10.1016/j.jtho.2019.08.426.

17. L. Shen, Z. H. Lu, J. Y. Wang, et al., "LBA52 Sintilimab Plus Chemotherapy Versus Chemotherapy as First-Line Therapy in Patients With Advanced or Metastatic Esophageal Squamous Cell Cancer: First Results of the Phase III ORIENT-15 Study," *Annals of Oncology* 32 (2021): S1330, https://doi.org/10.1016/j.annonc.2021.08.2132.

18. L. M. Sholl, F. R. Hirsch, D. Hwang, et al., "The Promises and Challenges of Tumor Mutation Burden as an Immunotherapy Biomarker: A Perspective From the International Association for the Study of Lung Cancer Pathology Committee," *Journal of Thoracic Oncology* 15 (2020): 1409–1424, https://doi.org/10.1016/j.jtho.2020.05.019.

19. Q. Wang, J. Gao, and X. Wu, "Pseudoprogression and Hyperprogression After Checkpoint Blockade," *International Immunopharmacology* 58 (2018): 125–135, https://doi.org/10.1016/j.intimp.2018.03.018.

20. S. Rosner, C. Liu, P. M. Forde, and C. Hu, "Association of Pathologic Complete Response and Long-Term Survival Outcomes Among Patients Treated With Neoadjuvant Chemotherapy or Chemoradiotherapy for NSCLC: A Meta-Analysis," *JTO Clinical and Research Reports* 3 (2022): 100384, https://doi.org/10.1016/j.jtocrr.2022.100384.

21. X. Wang, X. Wang, B. Hui, et al., "Efficacy of Neoadjuvant Chemo-Immunotherapy in Non-Small Cell Lung Cancer: A Real-World, Multicenter, Retrospective Study," *Translational Lung Cancer Research* 13 (2024): 849–860, https://doi.org/10.21037/tlcr-24-17.

22. J. Hu, L. Zhang, H. Xia, et al., "Tumor Microenvironment Remodeling After Neoadjuvant Immunotherapy in Non-Small Cell Lung Cancer Revealed by Single-Cell RNA Sequencing," *Genome Medicine* 15 (2023): 14, https://doi.org/10.1186/s13073-023-01164-9.

23. J. T. Leek, W. E. Johnson, H. S. Parker, A. E. Jaffe, and J. D. Storey, "The Sva Package for Removing Batch Effects and Other Unwanted Variation in High-Throughput Experiments," *Bioinformatics* 28 (2012): 882–883, https://doi.org/10.1093/bioinformatics/bts034.

24. W. D. Travis, S. Dacic, I. Wistuba, et al., "IASLC Multidisciplinary Recommendations for Pathologic Assessment of Lung Cancer Resection Specimens After Neoadjuvant Therapy," *Journal of Thoracic Oncology* 15 (2020): 709–740, https://doi.org/10.1016/j.jtho.2020.01.005.

25. M. I. Love, W. Huber, and S. Anders, "Moderated Estimation of Fold Change and Dispersion for RNA-Seq Data With DESeq2," *Genome Biology* 15 (2014): 550.

26. A. Subramanian, P. Tamayo, V. K. Mootha, et al., "Gene Set Enrichment Analysis: A Knowledge-Based Approach for Interpreting Genome-Wide Expression Profiles," *Proceedings of the National Academy of Sciences of the United States of America* 102 (2005): 15545–15550.

27. G. Yu, L.-G. Wang, Y. Han, and Q.-Y. He, "clusterProfiler: An R Package for Comparing Biological Themes Among Gene Clusters," *OMICS* 16 (2012): 284–287, https://doi.org/10.1089/omi.2011.0118.

28. A. Liberzon, "A Description of the Molecular Signatures Database (MSigDB) web Site," *Methods in Molecular Biology* 1150 (2014): 153–160, https://doi.org/10.1007/978-1-4939-0512-6_9.

29. A. M. Newman, C. L. Liu, M. R. Green, et al., "Robust Enumeration of Cell Subsets From Tissue Expression Profiles," *Nature Methods* 12 (2015): 453–457, https://doi.org/10.1038/nmeth.3337.

30. D. Aran, M. Sirota, and A. J. Butte, "Systematic Pan-Cancer Analysis of Tumour Purity," *Nature Communications* 6 (2015): 8971, https://doi.org/10.1038/ncomms9971.

31. D. Aran, Z. Hu, and A. J. Butte, "xCell: Digitally Portraying the Tissue Cellular Heterogeneity Landscape," *Genome Biology* 18 (2017): 220, https://doi.org/10.1186/s13059-017-1349-1.

32. J. Fu, K. Li, W. Zhang, et al., "Large-Scale Public Data Reuse to Model Immunotherapy Response and Resistance," *Genome Medicine* 12 (2020): 21, https://doi.org/10.1186/s13073-020-0721-z.

33. P. Charoentong, F. Finotello, M. Angelova, et al., "Pan-Cancer Immunogenomic Analyses Reveal Genotype-Immunophenotype Relationships and Predictors of Response to Checkpoint Blockade," *Cell Reports* 18 (2017): 248–262, https://doi.org/10.1016/j.celrep.2016.12.019.

34. H. Li, C.-W. Li, X. Li, et al., "MET Inhibitors Promote Liver Tumor Evasion of the Immune Response by Stabilizing PDL1," *Gastroenterology* 156 (2019): 1849–1861.e13, https://doi.org/10.1053/j.gastro.2019.01.252.

35. M. Ayers, J. Lunceford, M. Nebozhyn, et al., "IFN-γ-Related mRNA Profile Predicts Clinical Response to PD-1 Blockade," *Journal of Clinical Investigation* 127 (2017): 2930–2940, https://doi.org/10.1172/JCI91190.

36. C. S. Grasso, J. Tsoi, M. Onyshchenko, et al., "Conserved Interferon-γ Signaling Drives Clinical Response to Immune Checkpoint Blockade Therapy in Melanoma," *Cancer Cell* 38 (2020): 500–515.e3, https://doi.org/10.1016/j.ccell.2020.08.005.

37. J. J. Ishizuka, R. T. Manguso, C. K. Cheruiyot, et al., "Loss of ADAR1 in Tumours Overcomes Resistance to Immune Checkpoint Blockade," *Nature* 565 (2019): 43–48, https://doi.org/10.1038/s41586-018-0768-9.

38. D. H. Kaplan, V. Shankaran, A. S. Dighe, et al., "Demonstration of an Interferon Gamma-Dependent Tumor Surveillance System in Immunocompetent Mice," *Proceedings of the National Academy of Sciences of the United States of America* 95 (1998): 7556–7561.

39. S. J. Rodig, D. Gusenleitner, D. G. Jackson, et al., "MHC Proteins Confer Differential Sensitivity to CTLA-4 and PD-1 Blockade in Untreated Metastatic Melanoma," *Science Translational Medicine* 10 (2018): eaar3342, https://doi.org/10.1126/scitranslmed.aar3342.

40. J. W. Schoggins, S. J. Wilson, M. Panis, et al., "A Diverse Range of Gene Products Are Effectors of the Type I Interferon Antiviral Response," *Nature* 472 (2011): 481–485, https://doi.org/10.1038/nature09907.

41. P. K. Haber, F. Castet, M. Torres-Martin, et al., "Molecular Markers of Response to Anti-PD1 Therapy in Advanced Hepatocellular Carcinoma," *Gastroenterology* 164 (2023): 72–88, https://doi.org/10.1053/j.gastro.2022.09.005.

42. M. Reck, D. Rodríguez-Abreu, A. G. Robinson, et al., "Pembrolizumab Versus Chemotherapy for PD-L1-Positive Non-Small-Cell Lung Cancer," *New England Journal of Medicine* 375 (2016): 1823–1833.

43. M. Huang, J. O'Shaughnessy, J. Zhao, et al., "Association of Pathologic Complete Response With Long-Term Survival Outcomes in Triple-Negative Breast Cancer: A Meta-Analysis," *Cancer Research* 80 (2020): 5427–5434, https://doi.org/10.1158/0008-5472.CAN-20-1792.

44. J. L. Benci, L. R. Johnson, R. Choa, et al., "Opposing Functions of Interferon Coordinate Adaptive and Innate Immune Responses to Cancer Immune Checkpoint Blockade," *Cell* 178 (2019): 933–948, https://doi.org/10.1016/j.cell.2019.07.019.

45. L. Wang, Q. Jia, Q. Chu, and B. Zhu, "Targeting Tumor Microenvironment for Non-Small Cell Lung Cancer Immunotherapy," *Chinese Medical Journal Pulmonary and Critical Care Medicine* 1 (2023): 18–29, https://doi.org/10.1016/j.pccm.2022.11.001.

46. C. Lu, Z. Gao, D. Wu, et al., "Understanding the Dynamics of TKI-Induced Changes in the Tumor Immune Microenvironment for Improved Therapeutic Effect," *Journal for Immunotherapy of Cancer* 12 (2024): e009165, https://doi.org/10.1136/jitc-2024-009165.

47. R. Han, Y. Zhang, T. Wang, et al., "Tumor Immune Microenvironment Predicts the Pathologic Response of Neoadjuvant Chemoimmunotherapy in Non-Small-Cell Lung Cancer," *Cancer Science* 114 (2023): 2569–2583, https://doi.org/10.1111/cas.15778.

48. K. Mi, F. Chen, Z. Qian, et al., "Characterizing Heterogeneity of Non-Small Cell Lung Tumour Microenvironment to Identify Signature Prognostic Genes," *Journal of Cellular and Molecular Medicine* 24 (2020): 14608–14618, https://doi.org/10.1111/jcmm.16092.

49. H. Liu, X. Kuang, Y. Zhang, et al., "ADORA1 Inhibition Promotes Tumor Immune Evasion by Regulating the ATF3-PD-L1 Axis," *Cancer Cell* 37 (2020): 324–339, https://doi.org/10.1016/j.ccell.2020.02.006.

50. B. Wang, B. Jiang, L. Du, et al., "Tumor-Intrinsic RGS1 Potentiates Checkpoint Blockade Response via ATF3-IFNGR1 Axis," *Oncoimmunology* 12 (2023): 2279800, https://doi.org/10.1080/2162402X.2023.2279800.

51. S. Kumagai, Y. Togashi, T. Kamada, et al., "The PD-1 Expression Balance Between Effector and Regulatory T Cells Predicts the Clinical Efficacy of PD-1 Blockade Therapies," *Nature Immunology* 21 (2020): 1346–1358, https://doi.org/10.1038/s41590-020-0769-3.

52. X. Li, X. Zhou, Y. Li, et al., "Activating Transcription Factor 3 Promotes Malignance of Lung Cancer Cells In Vitro," *Thorac Cancer* 8 (2017): 181–191, https://doi.org/10.1111/1759-7714.12421.

53. J. Bar, M. S. Hasim, T. Baghai, et al., "Induction of Activating Transcription Factor 3 Is Associated With Cisplatin Responsiveness in Non-Small Cell Lung Carcinoma Cells," *Neoplasia* 18 (2016): 525–535, https://doi.org/10.1016/j.neo.2016.07.004.

54. C. St Germain, N. Niknejad, L. Ma, K. Garbuio, T. Hai, and J. Dimitroulakos, "Cisplatin Induces Cytotoxicity Through the Mitogen-Activated Protein Kinase Pathways and Activating Transcription Factor 3," *Neoplasia* 12 (2010): 527–538.

55. D. Fu, C. Wang, L. Yu, and R. Yu, "Induction of Ferroptosis by ATF3 Elevation Alleviates Cisplatin Resistance in Gastric Cancer by Restraining Nrf2/Keap1/xCT Signaling," *Cellular & Molecular Biology Letters* 26 (2021): 26, https://doi.org/10.1186/s11658-021-00271-y.

56. Y. Zhu, D. He, H. Bo, et al., "The MRVI1-AS1/ATF3 Signaling Loop Sensitizes Nasopharyngeal Cancer Cells to Paclitaxel by Regulating the Hippo-TAZ Pathway," *Oncogene* 38 (2019): 6065–6081, https://doi.org/10.1038/s41388-019-0858-7.

Supporting Information

Additional supporting information can be found online in the Supporting Information section.